Int. J. Heat Mass Transfer. Vol. 29, No. 2, pp. 227–240, 1986
Printed in Great Britain

0017-9310/86 $3.00 + 0.00

Convection in the vertical midplane of a horizontal cylinder. Comparison of two-dimensional approximations with three-dimensional results

P. BONTOUX,* B. ROUX,* G. H. SCHIROKY,†‡ B. L. MARKHAM†§ and F. ROSENBERGER†

* Institut de Mécanique des Fluides, CNRS-LA03, 1 Rue Honnorat, 13003 Marseille, France
† Department of Physics, University of Utah, Salt Lake City, UT 84112, U.S.A.

(*Received* 7 *May* 1984 *and in final form* 1 *August* 1985)

Abstract—Cylindrical, differentially heated and horizontal enclosures are commonly used in technological processes. A knowledge of the flow patterns in such a system is important for process optimization. In the past, flow predictions have often been made by using an asymptotic analytical approximation in the core, or by assuming a two-dimensional solution for the plane of symmetry. Laser Doppler anemometry studies, recently conducted by Schiroky and Rosenberger, have shown that in reality the free convection flows in the above configuration are highly three-dimensional. Here we compare the results for the vertical midplane obtained from the experiments and from 3-D numerical solutions with solutions of the aforementioned approximations. Both the core-driven and boundary layer-driven regimes are considered. In general the approximations give the correct Rayleigh-number-dependence of the velocities in the two regimes. However, the transition between the regimes and the magnitude and distribution of the velocity components were found to significantly depend on the 2-D approximation used.

1. INTRODUCTION

THE FREE convection in shallow rectangular cavities (boxes) and horizontal cylinders with differentially heated end walls has been studied experimentally, analytically and numerically by many workers. Part of this interest is due to the importance of these convective configurations in liquid- and vapor-phase crystal growth [1–4]. Analytical solutions for long rectangular cavities, based on a parallel flow approximation, were first proposed by Birikh [5], Hart [6], and Klosse and Ullersma [1]. The interaction between free convection and a net flow (forced diffusion) across cylindrical or two-dimensional (2-D) cavities was studied numerically by Rosenberger *et al.* [7–10]. Most of the recent work on free convection in closed shallow cavities is due to Bejan, Cormack, Imberger, Kimura, Shih, Tien *et al.* [11–20], Ostrach *et al.* [21, 22] and Hart [23]. The core flow theory of Bejan and Tien [14, 15] was extended to higher Rayleigh numbers with simplifying models for the flow near the end walls of 2-D cavities [24] and cylinders [25]. Experiments on rectangular cavities [26] and horizontal cylinders [25] have demonstrated the applicability of Gill's theory for free flow near vertical infinite plates [27] to the end regions of these confined geometries. Recently, laser Doppler anemometry studies [25] have shown that both in the core- and boundary-layer-driven regimes (CDR and BLDR) the flow in cylinders is highly three-dimensional, in contrast to the flow in rectangular boxes [17, 22]. Similar to the observations in boxes, however, it was found that the core flow in the cylinder tilts with respect to the horizontal on transition to the BLDR. Extensive 2-D numerical work has been aimed at predicting the transition between the two governing regimes [11, 19, 20, 28–30]. In our recent 3-D numerical modeling of free convection in cylinders [31] good agreement was obtained with the complex flow observed experimentally [25].

The aim of the present paper is a comparison of the flow characteristics for the CDR and BLDR in rectangular cavities and cylinders of aspect ratio $a = 5$ at $Pr = 0.73$. The aspect ratio is here defined as the horizontal length of the enclosure divided by the height of the heated end walls, i.e. $a = L/H$ and $a = L/2R_0$ for the rectangular cavity and cylinder, respectively. The comparison is based on the experimental, analytical and numerical results for the characteristic velocity distributions, the velocity boundary-layer thickness in the end regions and the temperature gradient in the core. Emphasis is put on the question of the validity of 2-D models for the flow in the vertical midplane of the cylinder. A similar comparison for tall rectangular boxes ($a < 1$) has been put forth by Mallinson and De Vahl Davis [32].

2. PHYSICAL MODELS

The two geometries of interest, a shallow rectangular cavity of height H and a cylinder with radius R_0, both of length L, are schematically depicted in Fig. 1(a). The vertical end walls are differentially heated to $\bar{T}_c$ and $\bar{T}_h$, with $\bar{T}_h > \bar{T}_c$. The horizontal walls are assumed to be perfectly conducting. The physical parameters that govern the flow are contained in the Prandtl number Pr

‡ Present address: GA Technologies, P.O. Box 85608, San Diego, CA 92138, U.S.A.
§ Present address: Naval Ocean Systems Center, San Diego, CA 92152, U.S.A.

NOMENCLATURE

a aspect ratio, $a = L/H$ or $L/2R_0$
b constant defined in Section 3.3, dimensionless
c Gill's free constant defined in Section 3.3, dimensionless
c constant defined in Section 3.2 for equation (7)
g gravitational acceleration [m s^{-2}]
h characteristic length in Ra, $h = H/2$ or R_0[m]
H height of rectangular enclosure [m]
k dimensionless parameter, equation (15)
k_1 core parameter (dimensionless axial temperature gradient)

$$k_1 = \frac{1}{2}\frac{\partial\theta}{\partial z} = \frac{H}{2\Delta T}\frac{\partial \bar{T}}{\partial \bar{z}} \quad \text{or} \quad \frac{R_0}{\Delta T}\frac{\partial \bar{T}}{\partial \bar{z}}$$

k_2 dimensionless constant, equation (9)
L length of the rectangular cavity of cylinder [m]
m dimensionless parameter, equation (15)
Pr Prandtl number, ν/κ
Q dimensionless parameter, equations (4) and (6)
$\bar{r}, r$ dimensional [m] and dimensionless radial position, $r = \bar{r}/R_0$
R_0 radius of cylinder [m]
Ra Rayleigh number, $\alpha g \Delta T h^3 Pr/\nu^2$
Ra_c critical Ra for transition from CDR to BLDR
$\bar{T}$ dimensional temperature [K]
$\bar{T}_h, \bar{T}_c$ temperatures at the hot and cold walls [K]
$\bar{T}_0$ reference temperature $1/2(\bar{T}_h + \bar{T}_c)$ [K]
ΔT $\bar{T}_h - \bar{T}_c$ [K]
$\bar{u}, \bar{w}$ velocity components in x-, z-directions [m s^{-1}]
$\bar{u}, \bar{v}, \bar{w}$ velocity components in r-, ϕ-, z-directions [m s^{-1}]
u, w dimensionless velocity components in x-, z-directions, $u = \bar{u}H/2\kappa$, $w = \bar{w}H/2\kappa$
u, v, w dimensionless velocity components in r-, ϕ-, z-directions, $u = \bar{u}R_0/\kappa$, $v = \bar{v}R_0/\kappa$, $w = \bar{w}R_0/\kappa$
$\bar{x}, \bar{z}$ position components [m]
x, z dimensionless position components, $x = 2\bar{x}/H$ or $\bar{x}/R_0$ and $z = 2\bar{z}/H$ or $\bar{z}/R_0$
$\hat{z}$ dimensionless axial position, equations (12) and (15).

Greek symbols

α coefficient of volumetric thermal expansion [K^{-1}]
β dimensionless vertical temperature gradient in the middle of the enclosure, $a\,\partial\theta/\partial x$
δ extent of end region, dimensionless
$\bar{\delta}$ characteristic flow thickness defined in Section 5.4 [m]
ε dimensionless function defined in Section 3.2
κ thermal diffusivity [m^2 s^{-1}]
γ dimensionless parameter, equation (5)
ν kinematic viscosity [m^2 s^{-1}]
ϕ azimuthal position component
ρ dimensionless parameter, equation (15)
θ dimensionless temperature, $2(\bar{T} - \bar{T}_0)/\Delta T$.

Subscripts

c critical
max maximum.

Superscripts

cond conduction regime
bl boundary-layer regime
2D, 3D Two- and three-dimensional.

Abbreviations

BLDR boundary-layer-driven regime
CDR core-driven regime.

and Rayleigh number Ra, based on a characteristic length h, which is taken as R_0 for the cylinder and $H/2$ for the cavity.

The coordinates $\bar{x}$ and $\bar{z}$ for the cavity are oriented vertically and along the symmetry axis, respectively, and are associated with the velocity components $\bar{u}$ and $\bar{w}$. The cylinder coordinates $\bar{r}$, ϕ and $\bar{z}$ are radially, azimuthally and axially oriented with the corresponding velocity components $\bar{u}$, $\bar{v}$ and $\bar{w}$. For the following analyses the coordinates and velocities are non-dimensionalized as defined in the Nomenclature. The vertical midplane, which is also the symmetry plane for the flow in the cylinder, is defined by $0 \leqslant r \leqslant 1$, $0 \leqslant z \leqslant 2a$, $\phi = 0$ and π [Fig. 1(a)]. The overall

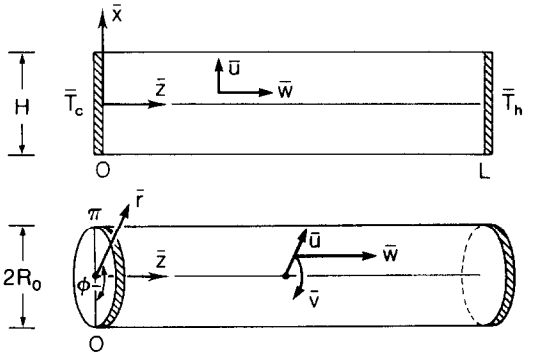

FIG. 1(a). Differentially heated horizontal, rectangular cavity and cylinder: definition sketch for dimensions, position coordinates and velocity components.

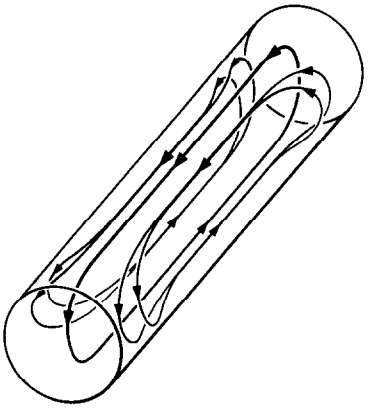

FIG. 1(b). Schematic presentation of overall flow pattern in differentially heated, horizontal cylinder.

characteristic of the flow, as derived from the experimental results [25] and an analysis of the computed solution [33], is schematically given in Fig. 1(b). One sees that in the end regions only part of the fluid flows along the cold (hot) vertical wall into the lower (upper) half of the cylinder. The remaining part changes the flow direction by dropping (rising) at the side wall over a considerable distance from the respective end wall.

3. ANALYTICAL MODELS

Analytical approximations for the velocity profile are available for the core of differentially heated rectangular cavities and cylinders. These approximations are based on temperature gradient parameters derived from experiments and analyses.

3.1. *Core flow velocities*

Parallel flow solutions, valid for the core of rectangular cavities and long cylinders, were proposed by Klosse and Ullersma [1], Birikh [5], Hart [6], and by Bejan and Tien [14, 15]. Elaborate approximations, allowing for secondary flows in cavities, were given by Cormack *et al.* [12]. The existence of these secondary flows was experimentally confirmed by Ostrach *et al.* [22]. Bejan and Tien [15] and Shih [18] included some interaction with the end regions. These core solutions are still limited to the S-shaped profile for the horizontal velocity component. Further improvements, which remove this limit for higher *Ra* conditions, are due to Tichy and Gadgil [24]. For cylinders, Schiroky and Rosenberger [25] proposed a third-order power series in *Ra* which well predicts the shift of the maximum in the core velocity towards the wall for the low *Ra*-range of the BLDR regime.

The analytical expressions for the core flow (horizontal velocity) used in our comparison are given in Table 1 and are numbered (1)–(3). They depend on the core parameter (axial dimensionless temperature gradient) k_1.

3.2. *Determination of* k_1

3.2.1. *For rectangular cavities.* For the CDR up to the beginning of the BLDR, Cormack *et al.* [12] derived an expression for k_1 in terms of Ra^2 and a [relation (4) in Table 2]. For the fully developed BLDR, Bejan and Tien [15] proposed a $Ra^{-3/5}$ dependence [relation (5)]. More recently, Hart [23] derived from Cormack *et al.*'s work an expression for k_1 that is valid for the whole CDR and BLDR range [relation (6)]. The expression is implicit but, for large values of *Ra*, one recovers the

Table 1. Analytical expressions for the dimensionless horizontal core velocity

Equation	Geometry	Power series approximations 1st order	3rd order	References
(1)	Rectangular cavity	$w^{2D}\ \frac{1}{6}k_1 Ra\,(x^2-1)x$		[1] [5] [6] [15]
(2)	Cylinder	$w^{3D}\ -\frac{1}{8}k_1 Ra\cos\phi(r^2-1)r$		[14]
(3)	Cylinder	$w^{3D}\ -\frac{1}{8}k_1 Ra\cos\phi(r^2-1)r$	$-\frac{(k_1 Ra)^3}{1{,}474{,}560 Pr}\left[\left(-\frac{143}{1680}r^{10}+\frac{3}{4}r^8-\frac{21}{40}r^6+\frac{125}{48}r^4-\frac{201}{140}r^2+\frac{4}{15}\right)r\cos\phi+\left(\frac{1}{28}r^8-\frac{1}{6}r^6+\frac{3}{10}r^4-\frac{1}{4}r^2+\frac{17}{210}\right)\times r^3\cos^3\phi\right]$	[25]

Table 2. Expressions for k_1

Equation	Regime	Approximation	Parameter	Wall condition	References
(4)	CDR and beginning of BLDR	$k_1 = \frac{1}{2a}(1-128Q\,Ra^2/a^3)$	$10^6Q = 1.74$	conducting	[12]
(5)	BLDR	$k_1 = 8.75\,\gamma^{1/10}Ra^{-3/5}$	$\gamma = 1.0$	insulating	[15]
(6)	CDR and BLDR	$1024Ra^2Qk_1^3 + 2ak_1 = 1$	$10^6Q = 1.70$–2.23	conducting	[23]

explicit relation

$$k_1 = (1024Q)^{-1/3}Ra^{-2/3},$$

which is independent of a, as Bejan and Tien's relation. Note that all these expressions, given in Table 2, depend on some adjustable parameters that are connected to some mean properties of the flow. Values of these parameters have been numerically obtained by the authors listed, by solving the 2-D governing equations with finite-difference techniques.

3.2.2. *For cylinders.* The end-integral method has been applied to the determination of k_1 in rectangular cavities by Bejan and Tien [15, 34]. Here we outline its application to the cylinder, for details see [35].

The governing equations in cylindrical coordinates are given in the literature [14, 18]. Assuming centro-symmetry and parallel flow in the core, the velocity field is given by $u = v = 0$ and the first-order power series term for w (Table 1). For the region at the cold end defined by $0 \leqslant z \leqslant \delta$, velocity profiles are assumed for u, v and w which obey the no-slip condition on the walls and match the core solution at the arbitrarily chosen $z = \delta$ with zero slope. The following profiles fulfill the continuity equation

$$u = \frac{3Ra\,k_1}{2\delta}\left(\frac{z}{\delta}-1\right)^2\frac{z}{\delta}(r-1)^2\cos\phi$$

$$v = \frac{3Ra\,k_1}{2\delta}\left(\frac{z}{\delta}-1\right)^2\frac{z}{\delta}(r-1)^2(r^2+2r-1)\sin\phi$$

$$w = -\frac{Ra\,k_1}{8}\left[3\left(\frac{z}{\delta}\right)^2-8\left(\frac{z}{\delta}\right)+6\right]\left(\frac{z}{\delta}\right)^2 \times(r^2-1)r\cos\phi. \quad (7a)$$

The temperature profile can then be written as

$$\theta = \left\{-\frac{Ra\,k_1^2}{81}\left(r^4-3r^2+2\frac{1+2c}{1+c}\right)r\cos\phi + 2k_2\right\}\varepsilon + 2k_1z - 1, \quad (7b)$$

where $\varepsilon = 1$ in the core, and in the end region

$$\varepsilon = \left(2-\frac{z}{\delta}\right)\frac{z}{\delta}. \quad (8)$$

The coefficient c in (7b) is zero for conducting walls and $c \to \infty$ for adiabatic walls. The thermal boundary conditions in the core (i.e. at $z = \delta$) are then matched with a slope related to k_1. For this one assumes the centro-symmetric temperature field

$$2k_2 = 1 - 2k_1a. \quad (9)$$

An integration of the energy equation over $0 \leqslant z \leqslant \delta$, $0 \leqslant r \leqslant 1$ and $0 \leqslant \phi \leqslant 2\pi$ then yields

$$0.00233Ra^2k_1^3 - 12.566k_2/\delta = 0. \quad (10)$$

After eliminating the pressure between the radial and axial momentum equation, and the azimuthal and axial momentum equations, respectively, the two resulting equations are combined to yield a unique momentum condition. Integration within the above limits then gives

$$0.8378k_1\delta + 2.0944k_2 - 0.6732k_1/\delta^3 = 0. \quad (11)$$

The integration of the energy and momentum equations was performed by using the algebraic computer language REDUCE [36]. While it is not

Table 3. Analytical expressions for the vertical flow

Equation	Solution	Regime	References
(12)	$u(\hat{z}) = \frac{k}{a}(\sin m\hat{z}\cosh m\hat{z} - \rho\cos m\hat{z}\sinh m\hat{z})$		[37] [38]
(13)	$u(z) = -\frac{a\,Ra}{12}z\left(\frac{z}{a}-1\right)\left(\frac{z}{a}-2\right)$	conducting (small Ra, $m \to 0$)	[37] [38]
(14)	$u(z) = -\sqrt{2}c^2Ra^{1/2}\sin\frac{mz}{a}e^{-mz/a}$ $\quad 0 \leqslant z \leqslant a$	boundary layer (high Ra, $m \gg 1$, $\beta = ab$)	[27]

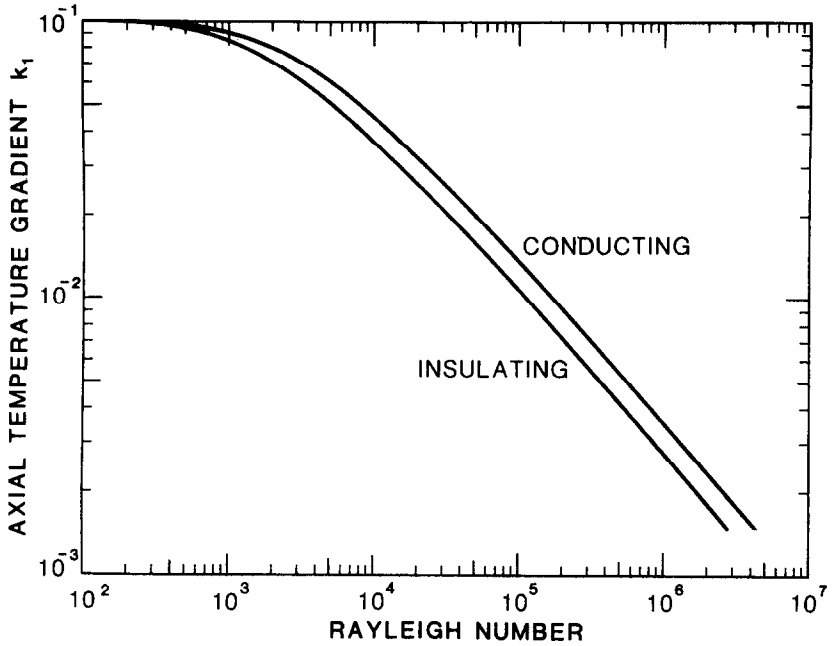

FIG. 2. Calculated dimensionless axial temperature gradient vs Rayleigh number for differentially heated cylinder with conducting and insulating walls, respectively.

possible to give an explicit expression for k_1, it can be numerically evaluated from equations (9)–(11). The resulting values of k_1 are plotted vs Ra in Fig. 2, for conducting and adiabatic conditions and $a = 5$. Shih [18] also attempted to calculate k_1 for the cylinder with the end-integral technique. However, his assumed velocity profiles for the end regions do not satisfy all boundary conditions and violate the continuity equation.

3.3. *Vertical flow along differentially heated walls*

Assuming steady-state parallel flow and weak vertical diffusion of temperature, Elder [37] has obtained the first similarity solution for free convection between two parallel vertical plates. The solution, denoted (12), is given in Table 3, together with the two asymptotic limits corresponding to the conduction regime [solution (13)], and the boundary-layer regime [solution (14)] obtained by Gill [27]. Following Vest and Arpaci [38] the new parameters in Table 3 are

$$\hat{z} = z/a - 1, \quad m = (a^3 \beta Ra/8)^{1/4},$$

$$k = -\frac{2m^2}{\beta}(\cos m \sinh m + \rho \sin m \cosh m)^{-1},$$

$$\rho = \tan m/\tanh m. \tag{15}$$

The solution (12) needs to be complemented by a relation between the thermal stratification parameter in the vertical direction, β and the aspect ratio a. From numerical results of Thomas and De Vahl Davis [39] and Roux *et al.* [40, 41] follows

$$\frac{\beta}{a} \approx 7.6 \times 10^{-4}(a^{4.25}Ra)^{1.75} \quad \text{for} \quad a^{4.25} \cdot Ra \lesssim 50$$

$$\frac{\beta}{a} \approx 0.8 \quad \text{for} \quad a^{4.25} \cdot Ra \gtrsim 50. \tag{16}$$

In (14) the coefficient c is a fitting parameter. From numerical results for a square cavity ($a = 1$), $c = 0.8$ [41]. From Elder's theory it follows that $c^2 = 1/2\sqrt{b}$, where b results from the boundary-layer relation $\beta/a = b$. From (16), $b = 0.8$ and, hence, $c = 0.748$.

4. EXPERIMENTAL AND NUMERICAL WORK

4.1. *Experimental data* [25]

Experimental results were obtained for a gas-filled cylinder with $a = 5$ ($R_0 = 1$ cm, $L = 10$ cm). The end wall temperatures were $\bar{T}_c = 27°C$ and $\bar{T}_h = 89°C$. The velocity field was determined by laser Doppler anemometry. The Rayleigh number was varied through the pressure and composition of the gas fill ($0.68 \leqslant Pr \leqslant 0.86$) from $74 \leqslant Ra \leqslant 1{,}283{,}000$. Centrosymmetry was observed for the velocity field within experimental resolution. This is somewhat at variance with our more recent measurements of the axial temperature distribution, that reveal a certain asymmetry between the hot and cold regions [31]. Such an asymmetry can be expected from the thermal expansion of the gas and/or variations of the physical properties as numerically shown for a rectangular cavity by Leonardi and Reizes [42], but can also be due to heat losses mainly at the hot end as shown by Leonardi [43].

Table 4. List of reported numerical methods

Method	Model	Governing hypotheses	Formulation	Method	References	Variables $(r, \phi, z)/(x, z)$
I	3D	Boussinesq; constant properties	vorticity, velocity	centered finite-differences Samarskii–Andreev scheme false transient	[45] [46] [30]	$9 \times 32 \times 33$, 65 uniform grid spacing
II	2D	Boussinesq; constant properties	vorticity, stream function	Hermitian finite-differences ADI scheme false transient	[47] [48] [41] [49]	21×41, 101 uniform grid spacing
III	2D	Boussinesq; constant properties	vorticity, stream function	pseudo-spectral-Tau-Chebyshev Adam–Bashforth/semi-implicit scheme; instationary	[50] [51] [52]	10×14 to 12×27, collocation points
IV	2D	Compressible; constant properties	primitive variables	TEACH method	[10]	16×32 two different uniform grid spacings

4.2. *Numerical methods*

The numerical works for rectangular cavities (2-D) and cylinders (3-D), that we will use in the comparison below, are listed in Table 4 together with the essential features of the approaches taken.

5. PRESENTATION AND DISCUSSION OF RESULTS

The governing parameter in all core-flow theories is the horizontal stratification parameter k_1. Hence, it will be discussed first. Although these theories become less and less meaningful as Ra increases, k_1 can still be considered as a variable that is characteristic for the thermal state in the enclosure. Then, we will discuss the Ra-dependence of the magnitude and profile of the velocities in the core and end regions, for which, at high enough Ra, one obtains boundary-layer behavior.

5.1. *Temperature gradient in the core*

The results for

$$k_1 = \frac{1}{2}\frac{\partial \theta}{\partial z}\left(= \frac{R_0}{\Delta T}\frac{\partial \bar{T}}{\partial \bar{z}} \quad \text{or} \quad \frac{H}{2\Delta T}\frac{\partial \bar{T}}{\partial \bar{z}}\right)$$

are plotted in Fig. 3. They refer to the experimental, analytical and numerical works listed in Table 5. The 3-D results for the cylinder correspond to $a = 5$, experimental details are given in [25, 35] and the computational approach is described in [31, 33]. The

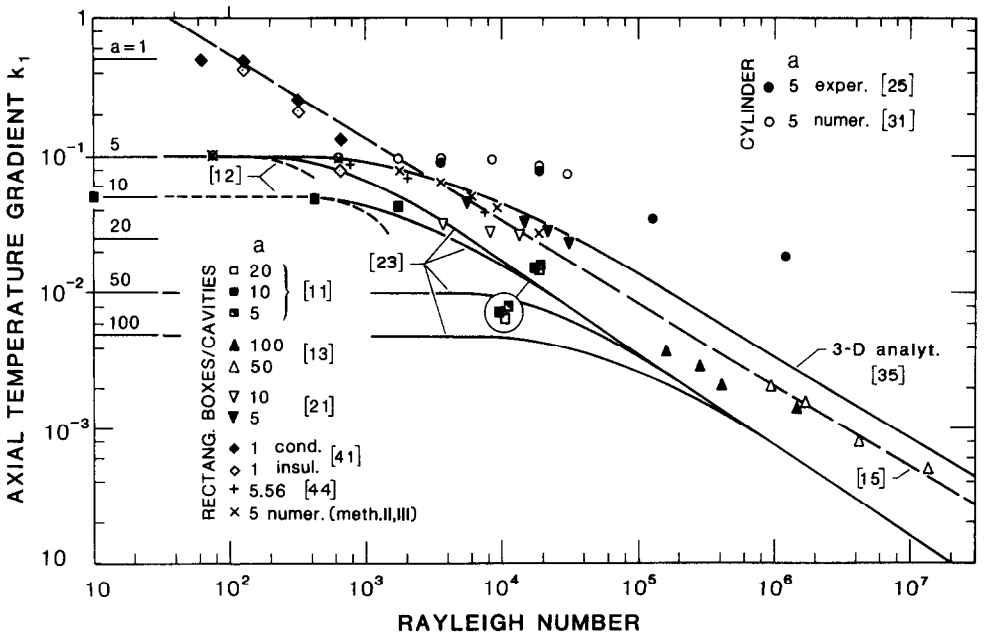

FIG. 3. Dimensionless axial temperature gradient vs Rayleigh number for cylinders and rectangular cavities of various aspect ratios: comparison of experimental, analytical and numerical results.

Table 5. Experimental, numerical and analytical determination of k_1

Geometry	Approach	Aspect ratio	Pr	References
Cylinder	experiments, numerical solutions, analytical solutions	5	0.68–0.85	[25] [31]
Rectangular box	experiments	50, 100	6.98	[13]
		5, 10	960, 1910	[21]
Rectangular cavity	analytical results	5, 10	—	[12]
		—	—	[15]
	computations	5, 10, 50, 100	—	[23]
		5, 10, 20	6.98	[11]
		5.56	0.526	[44]
		1	0.71	[41]

amount of data for the 2-D problem is much larger, with aspect ratios ranging from 100 to 1 and with Pr varying between 0.5 and 1900 [11, 13, 21, 41, 44].

The relations (4)–(6) given in Table 2 for the 2-D case are plotted in Fig. 3. A comparison of experiments and computations at large Ra shows fair agreement for the onset of the BLDR and the a-independence. The results for the transition to the BLDR for $a = 5$, 10 [11, 21] derived from (6) [23] approximate the experimentally and numerically obtained k_1s better than (4) [12]. In the fully-developed BLDR, the data obtained for $1 \leqslant a \leqslant 100$ lie roughly between the curves obtained from (5) and the explicit relation derived from (6) at large Ra in Section 3.2.1. The last result thus forms a lower limit for k_1 vs Ra.

For cylinders, the results derived from Section 3.2.2 for $a = 5$ with conducting side walls show that k_1 decreases much slower with increasing Ra than for the 2-D case. At a given Ra (in BLDR) the k_1 from the 3-D analytical estimate, [35] and Fig. 2, is about 1.6 times larger than from 2-D analysis. However, as compared to the 3-D numerical and experimental results, the 3-D analytical k_1 result is still roughly three times too small at $Ra = 18{,}700$. For $Ra < 30{,}000$ the experiments and numerical predictions agree quite well. Interestingly, the transition from CDR to BLDR occurs 'in reality' (3-D experiments and numerical modeling) at about 10 times higher Ra than in the 2-D systems. The value of k_1 is then 2–5 times larger than the k_1 derived from 2-D considerations.

5.2. *Velocity in the core region*

Analytical solutions for the maximum values of the horizontal velocity component w can be derived from (1) and (2), Table 1, respectively, as

$$|w_{\max}^{2D}| = \frac{Ra\, k_1}{9\sqrt{3}} \quad \text{at} \quad x = \pm\frac{1}{\sqrt{3}} \tag{17}$$

and

$$|w_{\max}^{3D}| = \frac{Ra\, k_1}{12\sqrt{3}} \quad \text{at} \quad r = \frac{1}{\sqrt{3}} \quad \text{for} \quad \phi = 0, \pi. \tag{18}$$

The relations (17) and (18), evaluated with the conduction condition $k_1 = (2a)^{-1}$ for $a = 5$, are plotted in Fig. 4 together with the experimental and numerical results. In addition, Fig. 4 contains plots of (18) and the corresponding relation derived from (3), both evaluated with the analytical values obtained for k_1 from (9)–(11); see also Fig. 2.

An analysis of these curves, together with the experimental and numerical data plotted in Fig. 4, results in the following observations:

(a) The experimental and 3-D numerical results (method I in Table 4) agree well over the whole range covered by the numerical data, i.e. $74 \lesssim Ra \lesssim 30{,}000$. The 2-D numerical results (methods II, III and IV), however, show significant deviations from these 3-D results, not only—as expected—in the CDR but also in the BLDR.

(b) The 2-D numerical 'compressible solutions' (method IV) are in good agreement with the solutions obtained from the Boussinesq approximations (methods II and III) in the range of Ra values for which computations were carried out.

(c) At low Ra (in the CDR) both 3-D analytical solutions, (2) and (3), yield good predictions. The 2-D solution (17), though correctly reflecting the linear dependence of $w_{\max}$ on Ra, overestimates the velocity by about 30% with respect to the cylinder; see the ratio of (17) and (18). This reflects the increased frictional interaction of the flow due to the relatively larger wall area of the cylinder.

(d) At high Ra (i.e. in the BLDR) the experimental and 3-D numerical results *for the core velocity* vary as $Ra^{1/2}$, parallel to Gill's boundary-layer relation (14) for u, see also Fig. 9. The velocity in the cylinder is about 1.5 times larger than the 2-D numerical solution, which, however shows a realistic Ra-dependence. The velocities obtained from the analytical solutions (18) and (3) with k_1s determined by (9)–(11), are too low. Their Ra-dependence is $Ra^{0.40}$ and $Ra^{0.44}$, respectively.

(e) If we define a critical Ra_c for the transition between CDR and BLDR, then we find from Fig. 4 that for $a = 5$, $Ra_c^{2D} \approx 2000$ whereas $Ra_c^{3D} \approx 6000$, i.e. a factor of about 3 between 2-D and 3-D behaviors.

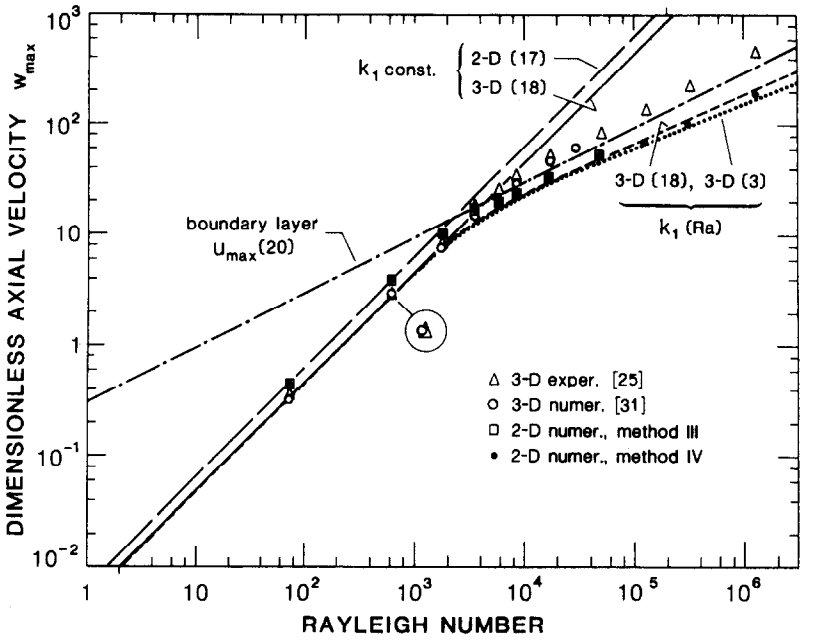

FIG. 4. Maximum value of dimensionless axial velocity (core velocity) vs Rayleigh number: comparison of experimental, analytical and numerical results.

The above points are further illustrated in a series of $w(r)$-profiles for discrete, increasing Ras in Figs. 5–8. In Fig. 5 one sees that in the CDR ($Ra = 660$) the 3-D analytical results, i.e. (2) and (3), agree well with the experimental and numerical values. The 2-D numerical values (methods II, III and IV in Table 4) lie too high.

At the upper end of the CDR ($Ra = 3580$, Fig. 6) the 2-D and 3-D numerical results are in very good agreement with experiment. The analytical predictions (2) and (3), based on k_1s obtained from (9)–(11), are too low. However, when (2) and (3) are evaluated with numerically obtained k_1s [31], agreement in magnitude is restored, with (3) yielding a more realistic distribution.

At $Ra = 8860$ (Fig. 7), the 2-D numerical and 3-D analytical velocity profiles differ strongly from each other and from experiment. Besides the different magnitudes, there are also distinctions into 'S-shapes' and 'Z-shapes'. At this Ra the analytical approaches are simply unable to yield realistic results either with analytically or numerically obtained k_1 values.

This trend is further emphasized by the results for $Ra = 18{,}720$ presented in Fig. 8. Yet it is noteworthy that the evolution of the Z-shape from the S-shape

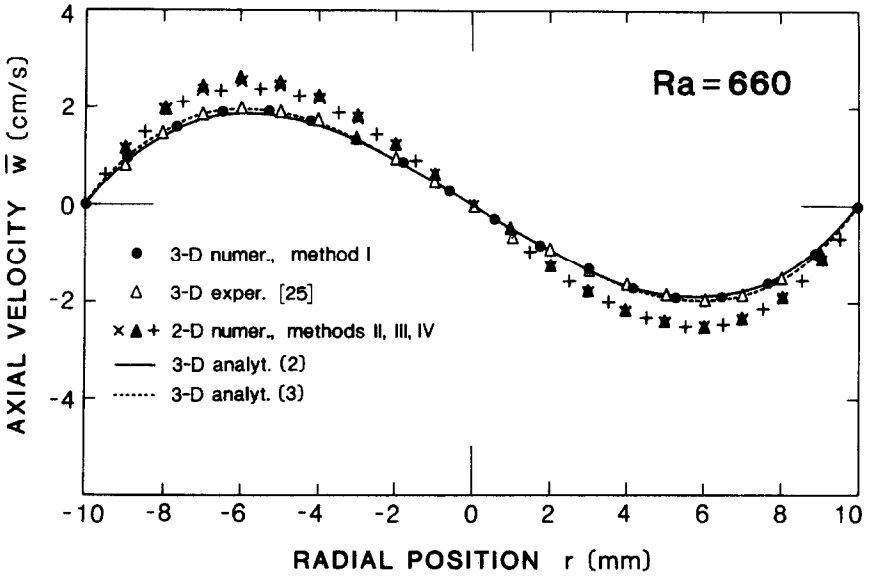

FIG. 5. Core velocity profiles for $Ra = 660$.

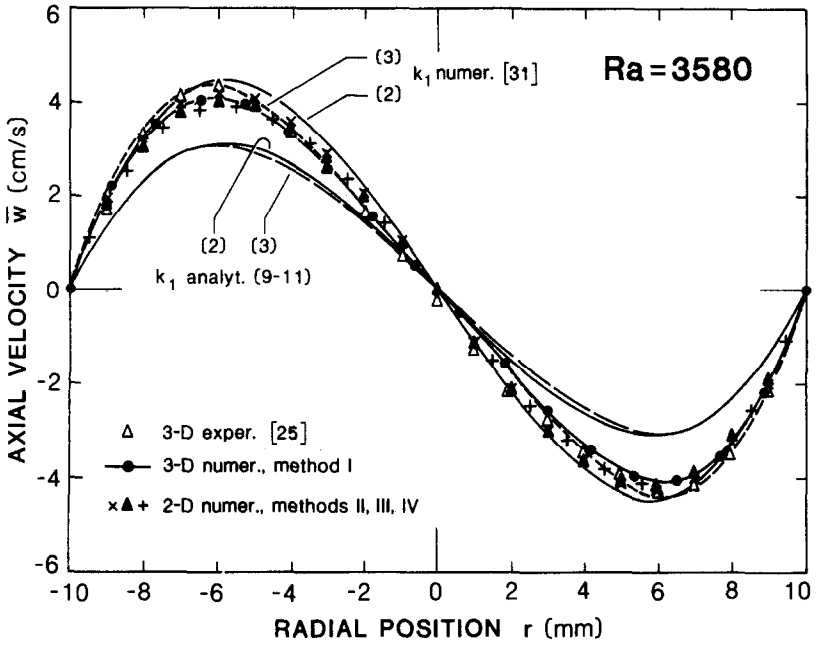

FIG. 6. Core velocity profiles for $Ra = 3580$.

(boundary-layer trend) occurs slower for 2-D than for 3-D solutions. For all four figures one should point out, however, the good agreement between experiment and 3-D numerical solutions obtained with only a $9 \times 32 \times 33$ mesh for r, ϕ and z, respectively.

5.3. *Velocity in the end regions*

Analytical solutions for the maximum of the vertical velocity component can be obtained from the limiting cases of Elder's general solution (12). From (13) and (14) of Table 3 we obtain for the conduction and boundary-

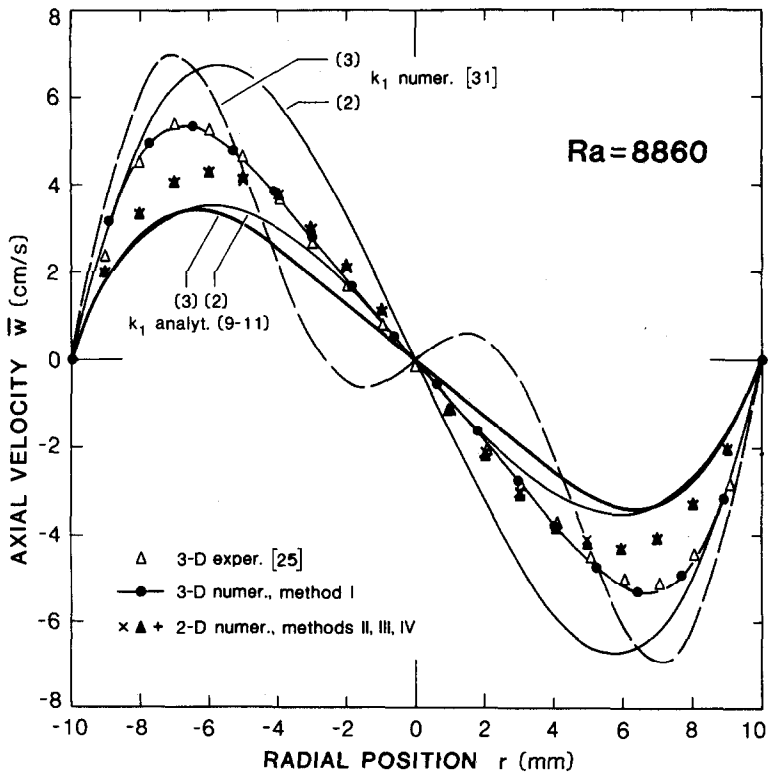

FIG. 7. Core velocity profiles for $Ra = 8860$.

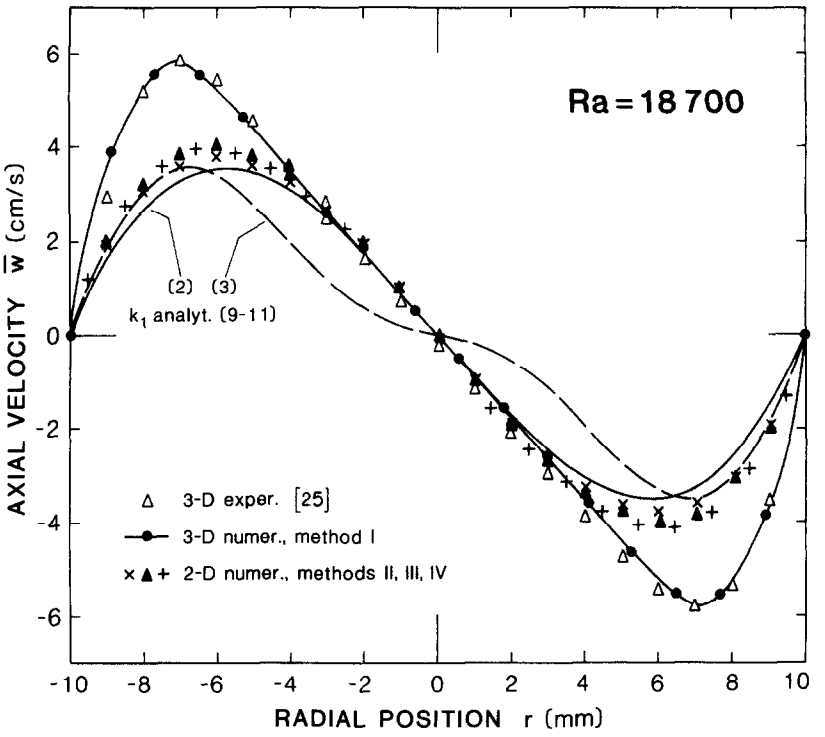

FIG. 8. Core velocity profiles for $Ra = 18{,}700$.

layer limit, respectively,

$$|u_{max}^{cond}| = a^2 Ra\sqrt{3}/54 \quad \text{at} \quad \frac{z}{a} = 1 \pm \frac{\sqrt{3}}{3} \tag{19}$$

and

$$|u_{max}^{bl}| = c^2 e^{-\pi/4} Ra^{1/2} \quad \text{at} \quad \Delta z = \pi c 2^{-3/4} Ra^{-1/4} \tag{20}$$

with $c = 0.8$.

These relations, together with the experimental and numerical results, are plotted in Fig. 9. An analysis of this figure reveals that

(a) experimental and 3-D numerical results agree fairly well in the CDR up to $Ra \approx 2000$ [see also (f) below];

(b) all results show a proportionality to Ra up to $Ra \approx 2000$, parallel to w_{max} obtained from (18), see also Fig. 4;

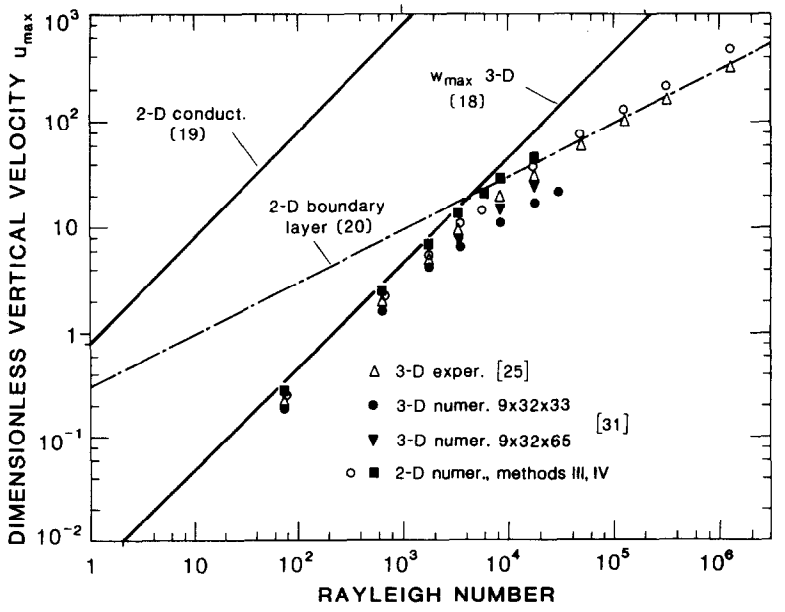

FIG. 9. Maximum value of dimensionless vertical velocity vs Rayleigh number: comparison of experimental, analytical and numerical results.

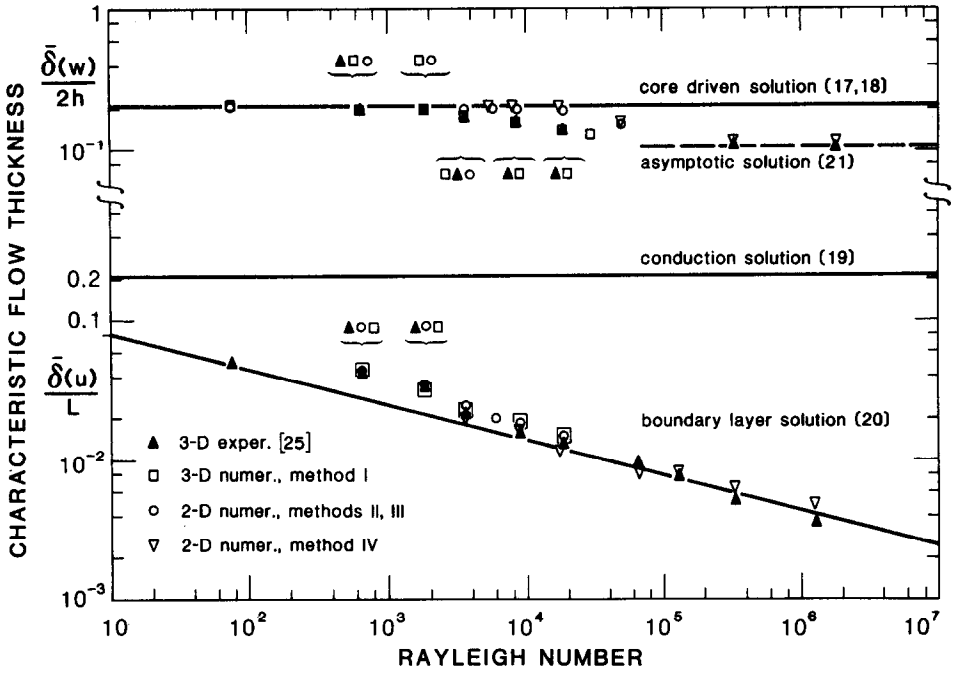

FIG. 10. Characteristic thickness of horizontal and vertical flow vs Rayleigh number, derived from experimental, analytical and numerical data.

(c) the 2-D numerical results that are based on the Boussinesq approximation lie throughout their range ($74 \lesssim Ra \lesssim 20{,}000$) considerably above the experimental cylinder values;

(d) the compressible solutions (method IV, Table 3) do not verify centro-symmetry but the difference does not exceed 5% in the end regions. Compressible results are below those for Boussinesq approximations over the entire range of Ra. This is to be compared with the reduction of the convection velocity observed by Leonardi [43] with the introduction of variable density and viscosity. Above $Ra = 10^4$ the compressible results have a dependence of $Ra^{0.55}$, thus slightly exceeding the dependence found for the 3-D results.

(e) above $Ra \approx 6000$ all results change from the linear behavior to an (approximate) $Ra^{1/2}$-dependence. (Note that the 3-D numerical results correspond to the first mesh point inside the cylinder, i.e. to a larger distance from the wall than the location of u_{max}, hence the low values.)

(f) the 2-D analytical relations (19) and (20) predict the transition to a boundary-layer-type flow to occur at Ra an order of magnitude too low.

An analysis of the experimentally determined velocity profiles $u(z)$ in the end region, was performed elsewhere [25]. It was found that at high Ras the shape and magnitude in the vertical midplane of the cylinder follow closely Gill's relation (14), i.e. they exhibit boundary-layer behavior.

5.4. *Characteristic flow thickness*

We define a characteristic flow thickness, $\bar{\delta}$ as the distance between a wall and the location of the maximum in the velocity component parallel to that wall. This parameter provides a different means of monitoring the transition from CDR to BLDR. For the end walls and side walls, respectively, we use the non-dimensionalized

$$\frac{\bar{\delta}(w)}{2R_0} \quad \text{or} \quad \frac{\bar{\delta}(w)}{H} \quad \text{and} \quad \frac{\bar{\delta}(u)}{L}.$$

Figure 10 shows these parameters evaluated from the experimental and numerical data together with plots of the analytical solutions (19)–(20). Also we show the asymptotic location of $\bar{\delta}(w)$ corresponding to (3) in the form

$$\frac{\bar{\delta}(w)}{2R_0} = 0.1065. \tag{21}$$

As can be expected from Figs. 5–8, the 3-D numerical characteristic flow thickness in the core agrees well with the experimental value up to the highest numerical point, $Ra = 30{,}000$. The velocity maximum is shifted towards the wall with increasing Ra. At very high Ras, the experimental $\bar{\delta}(w)$ tend towards the asymptotic relation (21) although the magnitude of the velocity maximum expected from (3) is much lower than the actual value; see e.g. Figs. 7 and 8. Also, for the 2-D numerical solution (17) the transition from the CDR occurs at higher Ra than for the 3-D solution.

The vertical thickness $\bar{\delta}(u)/L$ follows roughly a $Ra^{-1/4}$ trend, as predicted by Gill's analysis (20), both in the CDR and BLDR. This shows that in the end region the boundary-layer 'structure' sets in at rather low Ra, whereas the magnitude of the velocity maximum is still governed by the core mechanism up to $Ra \approx 2000$; see also Fig. 9. Note also that the 2-D and 3-D numerical solutions give similar values for $\bar{\delta}(u)/L$ although their values for the magnitude of the velocity are quite different.

6. CONCLUSIONS

The detailed comparison presented here shows that 2-D approximations can present the flow in the vertical midplane of a horizontal cylinder only rather poorly.

In the core driven flow regime both the core and the end region velocities are overestimated by typically 30%, although the location of w_{max} is well approximated.

In the boundary-layer driven regime, 2-D solutions show a more complex behavior:

(a) core velocities are underestimated by typically 40–50% and the velocity profile is only poorly approximated with too little shift of the maximum towards the wall;
(b) end velocities are overestimated by typically 30–40% with the actual velocity maximum again lying closer to the wall.

The Ra for the transition between core and boundary-layer mechanism for the core velocity is underestimated by the 2-D solutions; for an aspect ratio of $a = 5$ considered here, the values are $Ra_c^{2D} \approx 2000$ and $Ra_c^{3D} \approx 6000$. The *end velocity*, u, however, shows boundary-layer-like behavior throughout the whole Ra range investigated.

Acknowledgments—This work has been performed in collaboration between the Fluid Dynamics Group of the Université d'Aix Marseille II (IMFM-CNRS-LA03) and the Crystal Growth Laboratory (Department of Physics) of the University of Utah, within the frame of the CNRS-NSF Exchange Program (Grant G050252, P. Bontoux). We thank S. S. Leong and G. De Vahl Davis for permission to use their code CYL3D for the 3-D cylindrical configuration. The computations were carried out in France on the CRAY 01-Recherche of the CNRS (Paris) and the Cyber-750 of the CNES (Centre National d'Etudes Spatiales, Toulouse) and in the United States on the VAX-750 of the Department of Physics of the University of Utah. Research support by the CNRS and CNES, as well as by the National Science Foundation (Grant DMR 79-13183) and the Microgravity Sciences Program of the National Aeronautics and Space Administration (Grant NSG 1534) is gratefully acknowledged.

REFERENCES

1. K. Klosse and P. Ullersma, Convection in a chemical vapor transport process, *J. Cryst. Growth* **18**, 167–174 (1973).
2. J. R. Carruthers, Thermal convection instabilities relevant to crystal growth from liquids. In *Preparation and Properties of Solid State Materials* (Edited by W. R. Wilcox and R. A. Lefever), Vol. 3. Marcel Dekker, New York (1977).
3. A Solan and S. Ostrach, Convection effects in crystal growth by closed-tube chemical vapor transport. In *Preparation and Properties of Solid State Materials* (Edited by W. R. Wilcox), Vol. 4. Marcel Dekker, New York (1979).
4. S. M. Pimputkar and S. Ostrach, Convective effects in crystal growth from melt, *J. Cryst. Growth* **55**, 614–646 (1981).
5. R. V. Birikh, *J. appl. Math. tech. Phys.* **30**, 432 (1966).
6. J. E. Hart, Stability of thin non-rotating Hadley circulations, *J. atmos. Sci.* **29**, 687–697 (1972).
7. B. L. Markham, D. W. Greenwell and F. Rosenberger, Numerical modeling of diffusive–convective physical vapor transport in cylindrical vertical ampoules, *J. Cryst. Growth* **51**, 426–437 (1981).
8. B. S. Jhaveri, B. L. Markham and F. Rosenberger, On singular boundary conditions in mass transfer across rectangular enclosures, *Chem. Engng Commun.* **13**, 65–75 (1981).
9. B. S. Jhaveri and F. Rosenberger, Expansive convection in vapor transport across horizontal rectangular enclosures, *J. Cryst. Growth* **57**, 57–64 (1982).
10. B. L. Markham and F. Rosenberger, Diffusive-convective vapor transport across horizontal and inclined rectangular enclosures, *J. Cryst. Growth* **67**, 241–254 (1984).
11. D. E. Cormack, L. G. Leal and J. H. Seinfeld, Natural convection in a shallow cavity with differentially heated end walls. Part 2. Numerical solutions, *J. Fluid Mech.* **65**, 231–246 (1974).
12. D. E. Cormack, L. G. Leal and J. Imberger, Natural convection in shallow cavity with differentially heated end walls. Part 1. Asymptotic theory, *J. Fluid Mech.* **65**, 209–229 (1974).
13. J. Imberger, Natural convection in shallow cavity with differentially heated end walls. Part 3. Experimental results, *J. Fluid Mech.* **65**, 247–260 (1974).
14. A. Bejan and C. L. Tien, Fully developed natural counterflow in a long horizontal pipe with different end temperatures, *Int. J. Heat Mass Transfer* **21**, 701–708 (1978).
15. A. Bejan and C. L. Tien, Laminar natural convection heat transfer in a horizontal cavity with different end temperatures, *Trans. Am. Soc. mech. Engrs*, Series C, *J. Heat Transfer* **100**, 641–647 (1978).
16. S. Kimura and A. Bejan, Experimental study of natural convection in horizontal cylinder with different end temperatures, *Int. J. Heat Mass Transfer* **23**, 1117–1126 (1980).
17. A. Bejan, A. A. Al-Homoud and J. Imberger, Experimental study of high-Rayleigh-number convection in a horizontal cavity with different end temperatures, *J. Fluid Mech.* **109**, 283–299 (1981).
18. T. S. Shih, Computer-extended series: natural convection in a long horizontal pipe with different end temperatures, *Int. J. Heat Mass Transfer* **24**, 1295–1303 (1981).
19. G. S. Shiralkar and C. L. Tien, A numerical study of laminar natural convection in shallow cavities, *Trans. Am. Soc. mech. Engrs*, Series C, *J. Heat Transfer* **103**, 226–231 (1981).
20. G. S. Shiralkar, A. Gadgil and C. L. Tien, High Rayleigh number convection in shallow enclosures with different end temperatures, *Int. J. Heat Mass Transfer* **24**, 1621–1629 (1981).
21. A. Kumar and S. Ostrach, An experimental investigation of natural convection flows in rectangular enclosures of aspect ratio less than unity, FTAS/TR-77-132, Department of Mechanical and Aerospace Engineering, Case Western Reserve University (1977).
22. S. Ostrach, R. R. Loka and A. Kumar, Natural convection in low aspect-ratio rectangular enclosures. In *Natural*

Convection in Enclosures—HTD-8 (Edited by I. Catton and K. I. Torrance), pp. 1–10. ASME, New York (1980).
23. J. E. Hart, Low Prandtl number convection between differentially heated end walls, *Int. J. Heat Mass Transfer* **26**, 1069–1074 (1983).
24. J. Tichy and A. Gadgil, High Rayleigh number laminar convection in low aspect ratio enclosures with adiabatic horizontal walls and differentially heated vertical walls, *Trans. Am. Soc. mech. Engrs*, Series C, *J. Heat Transfer* **104**, 103–110 (1982).
25. G. H. Schiroky and F. Rosenberger, Free convection of gases in a horizontal cylinder with differentially heated end walls, *Int. J. Heat Mass Transfer* **27**, 587–598 (1984).
26. P. G. Simpkins and T. D. Dudderar, Convection in rectangular cavities with differentially heated end walls, *J. Fluid Mech.* **110**, 433–456 (1981).
27. A. E. Gill, The boundary-layer regime for convection in a rectangular cavity, *J. Fluid Mech.* **26**, 515–536 (1966).
28. R. A. Wirtz and W. F. Tseng, Natural convection across tilted, rectangular enclosures of small aspect ratio. In *Natural Convection in Enclosures*—HTD-8 (Edited by I. Catton and K. I. Torrance), pp. 47–54. ASME, New York (1980).
29. I. E. Lee and V. Sernas, Numerical study of heat transfer in rectangular air enclosures of aspect ratio less than one, ASME Paper 80-WA/HT-43, pp. 1–13 (1980).
30. J. C. Launay and B. Roux, Chemical vapor deposition: numerical models applied to transport of Ge by GeI_4 and GeI_2, *J. Cryst. Growth* **58**, 354–364 (1982).
31. C. Smutek, P. Bontoux, B. Roux, G. H. Schiroky, A. C. Hurford, F. Rosenberger and G. De Vahl Davis, Three dimensional convection in horizontal cylinders. Numerical solutions and comparison with experimental and analytical results, *Numer. Heat Transfer* **8**, 613–631 (1985).
32. G. D. Mallinson and G. De Vahl Davis, Three-dimensional natural convection in a box: a numerical study, *J. Fluid Mech.* **83**, 1–31 (1977).
33. C. Smutek, B. Roux, P. Bontoux and G. De Vahl Davis, 3-D Finite difference for natural convection in cylinders, In *Notes on Numerical Fluid Mechanics*, Vol. 7 (Edited by M. Pandolfi and R. Piva) pp. 338–345. Vieweg Verlag, Braunschweig (1983).
34. A. Bejan and C. L. Tien, Natural convection in horizontal porous medium subjected to an end-to-end temperature difference, *Trans. Am. Soc. mech. Engrs*, Series C, *J. Heat Transfer* **100**, 191–198 (1978).
35. G. H. Schiroky, Free convection of gases in a horizontal cylinder with differentially heated end walls—a study by laser Doppler anemometry. Ph.D. thesis, University of Utah, Salt Lake City, Utah (1982).
36. A. C. Hearn, REDUCE—a user oriented interactive system for algebraic simplification, *Proc. of the ACM-Symposium on Interactive Systems for Experimental Applied Mathematics*, Washington, D.C. (1967).
37. J. W. Elder, Laminar free convection in a vertical slot, *J. Fluid Mech.* **23**, 77–98 (1965).
38. C. M. Vest and V. S. Arpaci, Stability of natural convection in a vertical slot, *J. Fluid Mech.* **36**, 1–15 (1969).
39. R. W. Thomas and G. De Vahl Davis, Natural convection in annular and rectangular cavities—a numerical study, *Fourth Int. Congress Heat Transfer*, NC 2.4, Versailles, France (1970).
40. B. Roux, J. C. Grondin, P. Bontoux and G. De Vahl Davis, Reverse transition from multicellular to monocellular motion in vertical fluid layer. *Proc. Physico-Chemical-Hydrodynamics Conference* 3 (Edited by L. Van Gerven), Vol. 3F, pp. 292–297. European Physics Society Series, Madrid, Spain (1980).
41. B. Roux, J. C. Grondin, P. Bontoux and B. Gilly, On a high order accurate method for the numerical study of natural convection in a vertical square cavity, *Numer. Heat Transfer* **1**, 331–349 (1978).
42. E. Leonardi and J. A. Reizes, Natural convection in compressible fluids with variable properties. In *Numerical Methods in Thermal Problems* (Edited by W. Lewis and K. Morgan), pp. 297–306. Pineridge Press, Swansea (1979).
43. E. Leonardi, A numerical study of the effects of fluid properties on natural convection. Ph.D. thesis, University of New South Wales, Kensington, Australia (1984).
44. D. Manouélian, Convection thermique et solutale dans une enceinte fermée. Application à l'étude de l'aspect hydrodynamique de la croissance cristalline en phase vapeur, Mémoire, Conservatoire Nat. des Arts et Métiers, Aix en Provence, France (1982).
45. G. D. Mallinson and G. De Vahl Davis, The method of false transient for the solution of coupled elliptic equations, *J. comp. Phys.* **12**, 435–461 (1973).
46. S. S. Leong, Natural convection in cylindrical containers. Ph.D. thesis, University of New South Wales, Kensington, Australia (1981).
47. R. S. Hirsh, Higher order accurate difference solution of fluid mechanics problems by a compact differencing technique, *J. comp. Phys.* **19**, 90–109 (1975).
48. P. Bontoux, B. Forestier and B. Roux, Analyse et optimisation d'une méthode de haute précision pour la résolution des équations de Navier–Stokes instationnaires, *J. Méc Appl.* **2**, 1–26 (1978).
49. P. Bontoux, B. Gilly and B. Roux, Natural convection in cavities for high Rayleigh numbers. In *Notes on Numerical Fluid Mechanics*, Vol. 2 (Edited by E. H. Hirschell), pp. 22–35. Vieweg Verlag, Braunschweig (1979).
50. P. Bontoux, B. Bondet de la Bernardie and B. Roux, Spectral methods for solving unsteady 2-D Navier–Stokes equations in vorticity and stream-function formulation, GAMM-Workshop on Spectral Methods, Louvain-La-Neuve, Belgium (October 1980).
51. P. Bontoux, B. Bondet de la Bernardie and B. Roux, Spectral methods for natural convection problems. In *Numerical Methods in Coupled Problems* (Edited by E. Hinton, P. Bettess and R. W. Lewis), pp. 1018–1030. Pineridge Press, Swansea (1981).
52. F. Elie, A Chikahoui, A. Randriamampianina, P. Bontoux and B. Roux, Spectral approximation for Boussinesq double diffusion. In *Notes on Numerical Fluid Mechanics*, Vol. 7 (Edited by M. Pandolfi and R. Piva), pp. 57–64. Vieweg Verlag, Braunschweig (1983).

CONVECTION DANS LE PLAN MEDIAN D'UN CYLINDRE HORIZONTAL—COMPARAISON D'APPROXIMATIONS BIDIMENSIONNELLES AVEC LES RESULTATS TRIDIMENSIONNELS

Résumé—Des enceintes chauffées, horizontales cylindriques sont couramment utilisées dans l'industrie. La connaissance des configurations d'écoulement dans un tel système est importante pour l'optimisation du process. Dans le passé, les prédictions d'écoulement ont été souvent faites en utilisant une approximation analytique asymptotique dans le coeur, ou en supposant une solution bidimensionnelle pour le plan de symétrie. Des études d'anémonétrie Laser Doppler, récemment faites par Schiroky et Rosenberger, montrent que les écoulements de convection naturelle sont fortement tridimensionnels. On compare ici les résultats obtenus, pour le plan médian vertical, par les expériences et par les solutions numériques 3D, avec les approximations citées. On considère à la fois les régimes gouvernés par le coeur et ceux par la couche limite. En général, les approximations donnent la dépendance correcte des vitesses avec le nombre de Rayleigh dans les deux régimes. Néanmoins la transition entre les deux régimes, le module et la distribution des composantes de vitesse sont trouvés nettement dépendre de l'approximation 2D utilisée.

KONVEKTION AN DER SENKRECHTEN MITTELFLÄCHE EINES WAAGERECHTEN ZYLINDERS—VERGLEICH VON ZWEIDIMENSIONALEN NÄHERUNGEN MIT DREIDIMENSIONALEN ERGEBNISSEN

Zusammenfassung—Teilweise beheizte waagerechte zylindrische Hohlräume werden in technischen Prozessen oft eingesetzt. Die Kenntnis der Strömungsvorgänge in solchen Systemen ist wichtig für die Optimierung der Prozesse. Bisher wurden Strömungsberechnungen oft mit Hilfe eines analytischen asymptotischen Näherungsverfahrens im Kern oder unter Annahme einer zweidimensionalen Lösung für die Symmetrieebene durchgeführt. Messungen mit Laser-Doppler-Anemometern, die kürzlich von Schiroky und Rosenberger durchgeführt wurden, haben gezeigt, daß die Konvektionsströmungen bei der obigen Anordnung in Wirklichkeit ausgeprägt dreidimensional sind. Wir vergleichen hier Meßergebnisse und dreidimensionale Rechenergebnisse mit den Lösungen der oben genannten Näherungen. Sowohl Kern- als auch Grenzschichtbereiche werden betrachtet. Generell liefern die Näherungen die richtige Abhängigkeit der Rayleigh-Zahl von den Geschwindigkeiten in den beiden Bereichen. Das Übergangsgebiet zwischen beiden Bereichen sowie Betrag und Richtung der Geschwindigkeitskomponenten hängen jedoch entscheidend von der Art der zweidimensionalen Näherung ab.

КОНВЕКЦИЯ В СРЕДНЕМ КРУГОВОМ СЕЧЕНИИ ГОРИЗОНТАЛЬНО РАСПОЛОЖЕННОГО ЦИЛИНДРА. СРАВНЕНИЕ РЕЗУЛЬТАТОВ ТРЕХМЕРНЫХ РЕШЕНИЙ С РЕШЕНИЯМИ ДВУМЕРНОЙ ЗАДАЧИ

Аннотация—В технологических процессах обычно применяются цилиндрические горизонтальные полости с неравномерно нагреваемыми стенками. Знание режимов течения в такой системе важно для оптимизации процесса. Ранее расчеты течений проводились с помощью асимптотической аналитической аппроксимации в ядре или с применением двумерного решения в плоскости симметрии. Лазер-допплеровские анемометрические исследования, недавно выполненные Широким и Розернбергером, показали, что в действительности свободно-конвективные течения в указанных конфигурациях являются трехмерными. В настоящей работе экспериментальные результаты для среднего кругового сечения и данные, полученные из трехмерных численных решений, сравниваются с решениями, полученными из ранее упоминавшихся аппроксимаций. Рассматриваются режимы Течений в ядре потока и пограничном слое. В общем случае эти аппроксимации дают точную зависимость скоростей от числа Рэлея в указанных двух режимах. Однако, найдено, что переходной процесс между режимами, а также величина и распределение компонент скорости оказывают существенное влияние на свойства используемой двумерной аппроксимации.